J. At. Mol. Sci.
doi: 10.4208/jams.031313.062013a

Vol. **5** , No. 1 , pp. 9-20
February 2014

Density functional theory study of the catalytic reaction of N_2O ($^1\Sigma$) with CO ($^1\Sigma^+$) by Ni^+

Dong-Ping Chen[a], Ke Gai[a,*], Chao Kong[b], Yan-Xia Han[a], Li-Jie Hou[a], and Bo-Wang Wu[a]

[a] *College of Chemistry and Chemical Engineering, Longdong University, Qingyang 734000, China*
[b] *Lanzhou Institute of Chemical Physics, University of Chinese Academy of Sciences, Lanzhou 730000, China*

Received 13 March 2013; Accepted (in revised version) 20 June 2013
Published Online 18 November 2013

Abstract. The mechanism of the cyclic reaction CO($C_{\infty v}$,$^1\Sigma^+$) + N_2O($C_{\infty v}$,$^1\Sigma^+$)→ N_2 ($D_{\infty h}$,$^1\Sigma_g^+$) + CO_2($D_{\infty h}$,$^1\Sigma_g^+$) catalyzed by Ni^+ has been investigated on both double and quartet potential energy surfaces (PESs). The reactions were studied by the UB3LYP density functional theory. The calculated results of different spin PES show that the reaction proceeds in a two-step manner and spin crossing between different PES occurs. The involved crossing between the PES has been discussed by means of the intrinsic reaction coordinate approach used by Yoshizawa *et al.*, and the crossing points were located. Furthermore, the spin-orbit coupling (SOC) is calculated between electronic states of different multiplicities at the crossing points to estimate the intersystem crossing probabilities.

PACS: 31.15.Ew, 31.15.Qg

Key words: density functional theory, crossing point, molecule orbital(MO), natural bond orbital (NBO), spin-orbit coupling (SOC)

1 Introduction

It is generally known that the nitrous oxide impact is even more negative than CO_2 and methane effects toward the environment. N_2O is so steady to reach the troposphere, where it is responsible for the depletion of the ozone layer. Carbon monoxide is a significant toxic gas. How to reduce the environmental pollution resulted from N_2O and CO, which has been a hot subject for many experiments and theoretical calculations. Recently,

*Corresponding author. *Email address:* chendpldxy@126.com (D. P. Chen)

the catalytic reactions mechanism of CO with N_2O by Fe^+, Co^+ and Mn^+ were systematically investigated on potential energy surface using the quantum chemistry density functional theory [1-4]. Their research showed one oxygen atom of N_2O was directly extracted by metal ions to formate metal oxide ion. There does not exist NO insertion in all reaction process. The reactions of N_2O with Ge^+ and Se^+ were direct extracted oxygen mechanism using B3LYP/SDD+6-311+G(d) method by Chiodo *et al.* Additionally, the catalytic reactions mechanism of N_2O with CO by Pt^+ and CO with NO_2 by Sc^+ were studied using density functional method by Wang *et al.* [5-6]. Spin forbidden is an important factor to influence the reaction rate in gas phase reaction [7]. Many metal ions catalytic effect are not ideal because there is crossing and spin forbidden in different potential energy surfaces in their reactions. The reactions of Ti^+ (^{2}F and ^{4}F) with N_2O and Cu^+ (^{1}S and ^{4}D) with N_2O were investigated by Lv *et al.*[8] and Delabie *et al.*[9], respectively. They confirmed crossing phenomenon was existed in the export of reactions between potential energy surface. Experimental measurements are carried out by using an inductively coupled plasma/selected-ion flow tube (ICP/SIFT) tandem mass spectrometer, which tests the efficiency of many atomic cations to catalyze the activation of nitrous oxide by carbon monoxide [10-12].

While the experimental procedure and the rate coefficients for this kind of O-atom transport reactions are there for all to see, few theoretical researches were performed to compute the potential energy landscapes for the catalytic cycle, illustrated in the Scheme as follows:

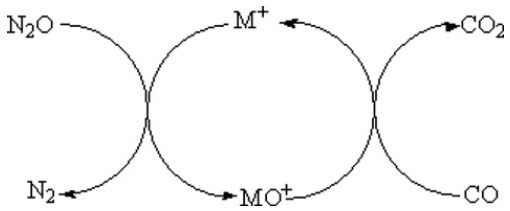

So far, 26 atomic cations were experimentally checked for their catalytic performance, but only ten activate nitrous oxide at room temperature[10]. Therefore, the theoretical study of the potential energy surface (PES) is the only tool to understand the reason of the catalytic efficiency about different cations. In our work, we considered the performance of Ni^+, which gives rise to a very slow reaction and it is insufficient information available about the energy profile for reaction to provide an explanation for its low O-atom transfer reactivity. Ni^+ reacts sufficiently quickly with N_2O to establish large enough concentrations of NiO^+ to obtain meaningful results for its reaction under experimental conditions with $k = 6.5 \times 10^{-13}$ cm$^3\cdot$ molecule$^{-1}\cdot$s^{-1}, but for the NiO^+ with CO the measured shown the rate coefficient could not be measured because NiO^+ could not be established in sufficient amounts[10].

In this paper we will report the detailed mechanisms of the reactions $Ni/N_2O/CO$ by using density functional theory. Calculated results are expected to calibrate experimental

results and to give some new suggestions that could not be reached experimentally under the laboratorial conditions.

2 Theoretical methods

The calculations were performed using the Gaussian03 program package[13]. At the indicated levels of theory, full geometry optimizations and frequency calculations were performed to verify the nature of the minima and evaluate zero-point energies. The fully optimized geometries and the vibrational frequencies have been determined using the spin-unrestricted three-parameter hybird[14] B3LYP density method[15], and a standardized 6-311G basis set was used together with polarization (2d) and diffuse (+) function[16]. All stationary points are characterized by vibrations are included. The transition state structures all represent saddle points, characterized by one negative eigenvalue of the hessian matrix. To ensure the reliability of the reaction path, the pathways between the transition structures and their corresponding minima have been characterized by the internal reaction coordinate (IRC) calculations [17-18].

The natural population analysis had been made by using the natural bond orbital (NBO)[19] option as implemented in Gaussian 03. In order to locate the crossing points (CPs) between the two potential energy surfaces (PESs) of different spin states, the procedure used by Heinemann *et al.* [20] was selected. We performed single-point energy calculations of the septet state as a function of the structural change along the IRC of the quintet state and vice versa [21-22].

Since in the case of the nickel catalyzed reaction we were interested also in the spin-orbit coupling (SOC) interaction which lend Approximate one-electron SOC calculations have been carried out with the GAMESS[23] suit of programs in the version of 2007, using the effective one-electron SO operator[24], in the following equation:

$$H_{SO}=\frac{\alpha^2}{2}\sum_i\sum_k\left(\frac{Z_K^*}{r_{ik}^3}\right)(S_i*L_{ik})=\sum_i h_i(Z^*)\frac{\alpha^2}{2}=\frac{e^2h}{4\pi m_e^2c^2}$$

where L_{ik} and S_i are the orbital and spin angular momentum operators for an electron i in the framework of the nuclei, indexed by K. To account for the missing two-electron part of the Hamiltonian, the nuclear charge Z_K is replaced by an effective parameter, Z_K^*, which can be taken as the screened nuclear charge.

3 Results and discussion

The optimized geometries of stationary points and the potential energy profiles of the two reactions are displayed in Figs. 1, 2 and Table 1, respectively. For all cited single-point energies are performed with UB3LYP/6-311++G(3df,3pd)[25], zero-point energy (ZPE) corrections are included. An analysis of the B3LYP molecular orbitals reveals the

Table 1: Vibrational frequencies (in cm^{-1}) for the transition states and energy of various compounds in the reaction.

Species	E_T/Hartree	E_R(kJ·mol^{-1})	Freq(cm^{-1})	Species	E_T/Hartree	E_R(kJ·mol^{-1})	Freq(cm^{-1})
$^2Ni^+$+N_2O(CO)	-1806.0507	0.00		$^4Ni^+$+N_2O(CO)	-1806.0049	120.5	
^{2}IM1(CO)	-1806.0863	-93.3		^{4}IM1(CO)	-1806.0303	53.6	
^{2}TS1/2(CO)	-1806.0268	62.9	-667.1	^{4}TS1/2(CO)	-1806.0002	132.7	-1561.5
^{2}IM2(CO)	-1806.0516	-2.3		^{4}IM2(CO)	-1806.1071	-148.1	
$^2NiO^+$+N2(CO)	-1806.0210	78.0		$^4NiO^+$+N_2(CO)	-1806.0381	33.1	
^{2}IM3(N_2)	-1806.0875	-96.6		^{4}IM3(N2)	-1806.1223	-188.0	
^{2}TS3/4(N_2)	-1806.0829	-84.4	-379.1	^{4}TS3/4(N_2)	-1806.0691	-48.2	-548.4
^{2}IM4(N_2)	-1806.2243	-455.7		^{4}IM4(N_2)	-1806.1079	-150.1	
$^2Ni^+$+CO_2(N_2)	-1806.1883	-361.3		$^4Ni^+$+ CO_2N_2	-1806.1424	-240.7	

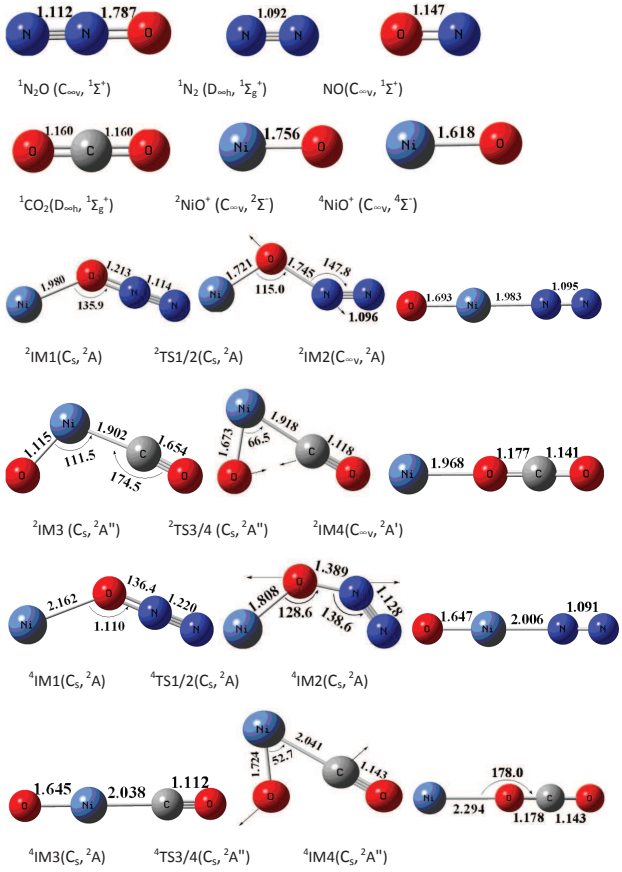

Figure 1: Optimized geometries of various species in reaction. (bond length in Å, bond angles in degree).

important orbital interactions at the initial complexes, which are shown in Fig. 3 and Fig. 4. In Fig. 5 the structure of CP are schematically depicted. The favorable PES of the energetic values obtained and frontier molecular orbital of CP2 are shown, respectively in Figs. 6. The calculated natural population analysis for the stationary points are collected in Table 2.

Table 2: NBO and electron configuration of the Ni atom at the UB3LYP/6-311+G(2d) level.

The analysis of the Second-Order Perturbation Theory						
Species (Ni)	The values of the NBO charge	The electron configuration of Ni	Donor NBO(i)	Acceptor NBO(j)	E(2)kJ/mol	$n_i \rightarrow \sigma_j^*$
^{2}IM1	0.963	$4S^{0.04}3d^{4.97}$	LP O	BD* N_1-N_2	139.8	$n_O \rightarrow \sigma^*_{N_1-N_2}$
^{2}TS1/2	1.228	$4S^{0.09}3d^{4.94}4p^{0.01}$	LP N_1	BD* O-Ni	110.2	$n_{N_1} \rightarrow \sigma^*_{O-Ni}$
^{4}IM2	1.180	$4S^{0.16}3d^{4.94}5p^{0.01}$	LP O	LP* Ni	152.4	$n_O \rightarrow \sigma^*_{Ni}$
^{4}IM3	1.097	$4S^{0.19}3d^{4.94}5p^{0.01}$	LP O1	LP* Ni	151.5	$n_{O_1} \rightarrow \sigma^*_{Ni}$
			LP C	LP* Ni	146.7	$n_C \rightarrow \sigma^*_{Ni}$
$^{2/4}$CP2	1.220	$4S^{0.18}3d^{8.58}4p^{0.01}$	LP C	BD* Ni-O_2	121.7	$n_c \rightarrow \sigma^*_{Ni-O_2}$
			LP C	LP* Ni	109.0	$n_c \rightarrow n^*_{Ni}$
^{2}TS3/4	1.120	$4S^{0.11}3d^{4.59}$	LP C	BD* Ni-O_1	300.0	$n_C \rightarrow \sigma^*_{Ni-O_1}$
^{2}IM4	0.985	$4S^{0.04}3d^{4.96}$	LP O_1	BD* O_2-C	206.6	$n_{O_1} \rightarrow \sigma^*_{O_2-C}$

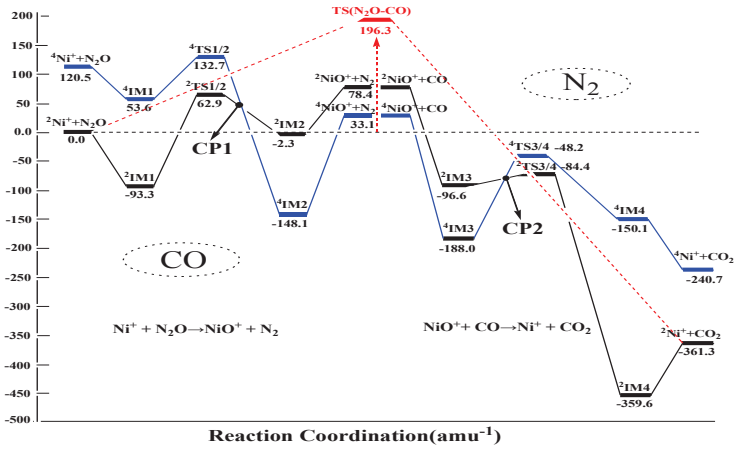

Figure 2: Double and quartet energy surfaces for the reactions: N_2O with CO catalyzed with Ni^+.

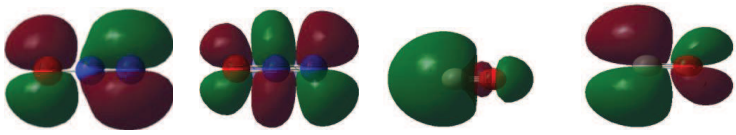

Figure 3: The HOMO and LUMO orbits of N_2O(a and b) and CO(c and d) molecules.

3.1 Overall of the Stationary Points

Before evaluating the influence of the Ni^+ on the kinetic features of the process, we analyzed the reaction path relating to the reduction of N_2O by CO in the absence of any catalyst. In this case, the reactive process to evaluate is the following:

$$CO(C_{\infty vf},{}^1\Sigma^+)+N_2O(C_{\infty v},{}^1\Sigma)\rightarrow N_2(D_{\infty h},{}^1\Sigma_g^+)+CO_2(D_{\infty h},{}^1\Sigma_g^+) \quad (1)$$

According to our calculations, the uncatalyzed reduction (1) shown in the top profile proceeds (the red color in Fig. 2) in one step via a high activation barrier of 196.3 kJ·mol^{-1} and is strongly exothermic, by 361.3 kJ·mol^{-1} according to the calculations. The potential energy curve, computed at the same level of the theory by Böhme *et al.* shows $E^{\neq}$ =197.6 kJ·mol^{-1}, and $\Delta_r H$= -362.8 kJ·mol^{-1}[12]. The structure of the transition state (in Fig. 1) corresponds to a direct attack of oxygen atom of N_2O on the carbon atom of CO. The N-O bond is being broken, and the C-O bond is being formed.

For the Ni^+ catalyst, the reaction mechanism is summarized as follow:

$$Ni^+(^2D,^4F)+N_2O(C_{\infty v},^1\Sigma^+)\rightarrow NiO^+(^1\Sigma^-,^4\Sigma^-)+N_2(D_{\infty h},^1\Sigma_g^+) \quad (2)$$

$$NiO^+(^2\Sigma^-,^4\Sigma^-)+CO(C_{\infty v},^1\Sigma^+)\rightarrow Ni^+(^1D,^4F)+CO_2(D_{\infty h},^1\Sigma_g^+) \quad (3)$$

The Ni^+ is first considered in its ground state, ^{2}D ($3d^9$) owing to the fact that the first excited state of this ion lies at a higher energy. The Ni^+ ^{4}F ($3d^84s^1$) electronic configuration is found 120.5 kJ·mol^{-1} above the corresponding ground state.

In Figs. 1 and 2, the reaction (2) is the formation of [Ni-NNO]$^+$ complexes on both ground (^{2}M1, C_s) and excited-state (^{4}IM1, C_s) PESs for the interaction of Ni^+ (X^2D, $3d^9$;^{4}F, $3d^84s^1$) and N_2O. From the NBO analyses of charge distribution, about the $^{2/4}$IM1, the positive charge of this Ni atom decreases to 0.963 and 0.933, respectively, and a small electronic charge transfer takes place from N_2O fragment to the Ni ion (see Table 2). So we can see that the $^{2/4}$IM1 complexes are very weak, in which the N_2O molecule remains almost the linear structure (the O-N-N angle is about 180.0°), and they have Cs symmetry. From the $^{2/4}$IM1, the next step is associated with nickel transfer process between the N_1(N_1 indicates the frist N atom, the others are the same means) and O atom, to yield the $^{2/4}$IM2, via transition states, $^{2/4}$TS1/2. In this process, although the transition structures on the double and quartet surfaces are also planar (Cs symmetry), the N_2O structure changes are much bigger, which means the N_2(N_2 indicates the second N atom) is gradually bent outward, away from the Ni. The imaginary frequency characterizing the $^{2/4}$TS1/2, having the value of -667.1 cm^{-1} and -1561.5 cm^{-1} in double and quartet state respectively, corresponds to the stretching vibrational mode indicating the formation of the new Ni-O bond and the breaking of the N-O bond. The corresponding bond Ni-O distances gradually increase to about 1.983 Å and 2.006 Å in $^{2/4}$IM2, respectively. Finally the separated products, NiO^+ + N_2, can be obtained directly from $^{2/4}$IM2 product complexes, overcoming a barrier height of 132.7 kJ·mol^{-1} and 62.9 kJ·mol^{-1}, respectively. About the reaction (3), as described in Figs. 1 and 2, the reactivity patterns of the double or quartet PESs are similar, and both involve initial attack of NiO^+ ($X^4\Sigma^-$, $^2\Sigma^-$) to the CO to form the corresponding [ONi-CO]$^+$ complexes with binding energies of -188.0 kJ·mol^{-1} (^{4}IM3) and -96.6 kJ·mol^{-1} (^{2}IM3). The imaginary frequency characterizing the $^{2/4}$TS3/4, having the value of -379.1 cm^{-1} and -548.4 cm^{-1} in double and quartet state respectively, corresponds to the stretching vibrational mode indicating the formation of the new C-O bond and the breaking of the Ni-O bond. The corresponding bond Ni-O distances gradually increase to about 1.968 Å and 2.294 Å in $^{2/4}$IM4, respectively. Finally the

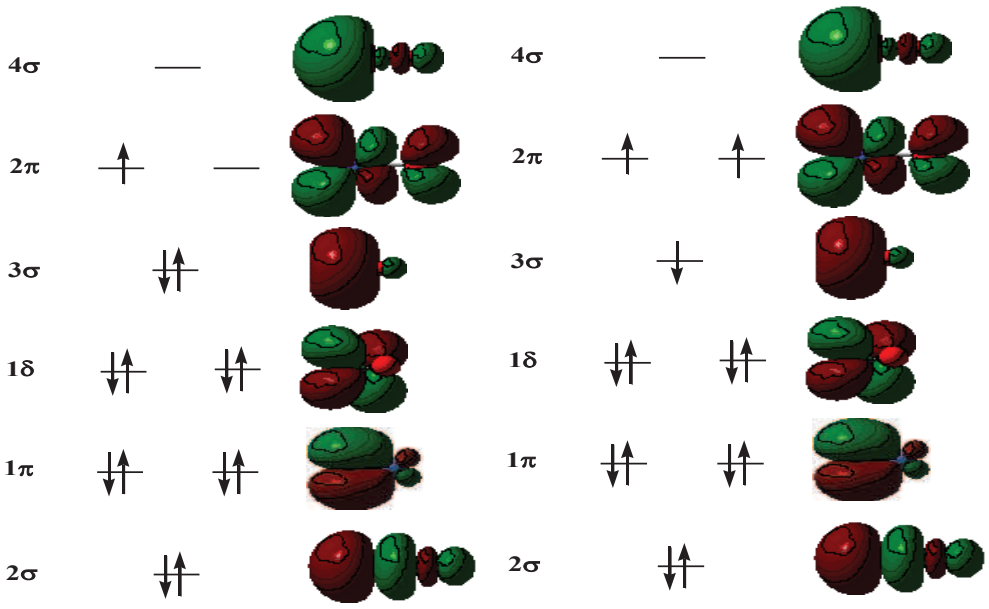

(a) $^{2}NiO^{+}(^{2}\Sigma^{-})$ (b) $^{4}NiO^{+}(^{4}\Sigma^{-})$

Figure 4: The molecule orbital of $^{2-4}NiO^{+}$.

separated products, $Ni^{+} + CO_2$, can be obtained directly from $^{2/4}$IM4 product complexes, overcoming a barrier height of -48.2 kJ·mol^{-1} and -84.4 kJ·mol^{-1}, respectively.

3.2 Theoretical mechanism

3.2.1 Orbital aspects

An analysis of molecular orbital at the UB3LYP/6-311+G(2d) level reveals the important orbital interactions at the initial complexes, which are shown in Fig. 3 and Fig. 4. The molecular orbital of N_2O show that the HOMO is a 2π-orbital which is anti-bonding with the N-O bond but bonding to the N-N bond (see Fig. 3a). The LUMO is a $3\pi^{*}$-orbital with anti-bonding character for the N-O and N-N bonds (see Fig. 3b). As in the $^{2-4}$IM1, the O-N_1-N_2 system remains linear, but the Ni-O-N_1 angle is bent. These structural parameters can be rationalized by looking at the orbital interactions between the $^{2}Ni^{+}$ ($X^{2}D$, $3d^{9}4s^{0}$) ion and N_2O, shown in Fig. 4a. Apart from a small electrostatic force and polarization terms, the primary reason for the bent Ni-O-N_1 angle is a σ electron donating interaction between the N_2O HOMO and the $^{2}Ni^{+}$ $3d_z^2$ orbital. On the other hand, the interaction between the $^{2}Ni^{+}$ 4s orbital and in-plane N_2O LUMO, which could bring about back-donation, is still weak in the initial complex. Additionally, the Ni-O bond length of ^{2}IM1 is shorter than in the excited state Ni-O bond of ^{4}IM1, because of the absence of 4s-ligand repulsion. The molecular orbitals of CO show that the HOMO is a 2σ-orbital which is

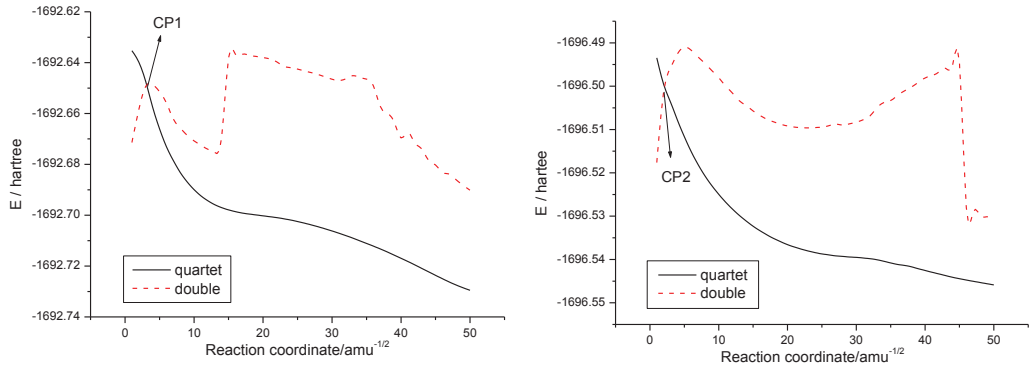

Figure 5: Potential energies curve-crossing points diagram: (a) along the quartet state IRC, (b) along the quartet state IRC.

anti-bonding with respect to the C-O bond (see Fig. 3c), and the LUMO is a $2\pi^*$-orbital with anti-bonding character for the C-O bond (Fig. 3d). As shown in Fig. 4c, the lowest-lying valence orbitals of $^2NiO^+(^2\Sigma^-,2\sigma^21\pi^41\delta^43\sigma^22\pi^14\sigma^0)$ ions LUMO (2π) and HOMO (2π) interact mainly with the CO HOMO (2σ) and LUMO ($2\pi^*$), respectively. The result of interaction is which ^{2}IM3 is curving structure and the angle of C-Ni-O_2 is 111.5°. Fig. 4 d also shows the lowest-lying valence orbitals of $^4NiO^+(^4\Sigma^-,2\sigma^21\pi^41\delta^43\sigma^12\pi^24\sigma^0)$ ion are the 2σ and 1π orbitals. The 2σ and 1π orbitals have significant electron density on both atoms and strongly bonding. Above these, but very close in energy, lie the nonbonding metal-centered $1\delta3\sigma$ orbitals and the weakly anti-bonding 2π. The lowest-unoccupied molecular orbital (4σ) is mostly anti-bonding. So the LUMO (4σ) of 4NiO+ interact mainly with the CO HOMO (2σ) and the HOMO (2π) of $^4NiO^+$ interact mainly with the CO LUMO ($2\pi^*$). The result of interaction is that ^{4}IM3 is linear structure. According to the above orbital analysis, the conclusion we have drawn is in agreement with the theoretical results which we have counted.

3.2.2 Charge aspects

To emphasize the importance of charge transfer, the results of the natural bond orbital analysis for some stationary points are showed in Table 2. On the basis of orbital analysis above, the Ni^+ ion and N_2O, the NiO^+ ion and CO firstly form a reactant complex 2/4IM1 and 2/4IM3, respectively. In this step, the NBO analysis show that the values of the NBO charge of Ni in double state are from 0.963 (IM1) to 1.227 (IM2), 1.052 (IM3) and then to 0.985 (IM4), while in quartet state the values of the NBO charge of Ni are are from 0.933 (IM1) to 1.180 (IM2), 1.097 (IM3) and then to 0.984 (IM4). To further understand more detailed information on the net charge transfer (CT) processes can be estimated by second-order perturbation theory $(E(2) = -2 < \sigma|\check{E}|\sigma^* > /\varepsilon_{\sigma^*} - \varepsilon_\sigma)$ [26]. In the ^{2}IM1, $n_O \rightarrow \sigma^*_{N_2-N_2}$ (n_O indicates the lone pair of the O atom, the others are the same means) in-

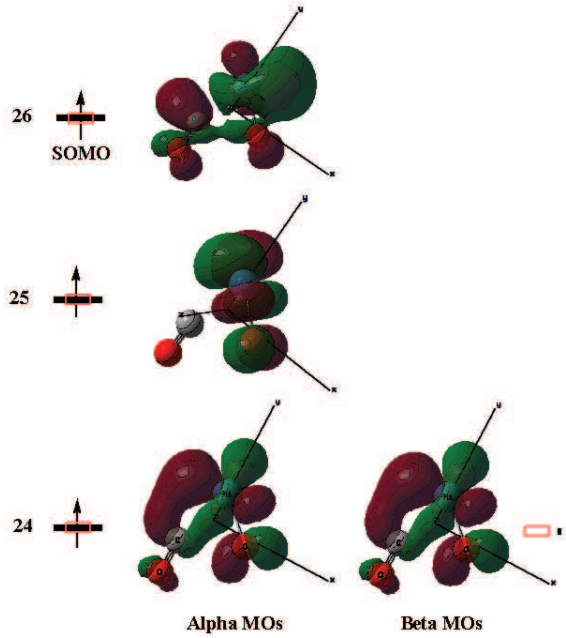

Figure 6: Frontier molecular orbital interaction analyzes for CP2.

teraction between the oxygen lone pair and the N_1-N_2 anti-bond orbit is seen to give the strongest stabilization, 139.8 kJ·mol^{-1}. In the ^{2}TS1/2, the intermolecular CT occurs importantly between the lone pair of N_1(electron donor) and the Ni-O anti-bond $n_O \rightarrow \sigma^*_{O-N_i}$, corresponding to the second-order perturbation energies, $E(2)$, 110.2 kJ·mol^{-1}. In the ^{4}IM2, $n_O \rightarrow \sigma^*_{N_i}$ interaction between the oxygen lone pair and the atomic empty orbit of Ni is seen to give the strongest stabilization, 152.4 kJ·mol^{-1}. In the ^{4}IM3, $n_C \rightarrow \sigma^*_{Ni}$, $n_{O_1} \rightarrow \sigma^*_{Ni}$ interaction between the C, O_1 lone pairs and the atomic empty orbits of Ni are seen to give the strongest stabilization, 146.7 kJ·mol^{-1} and 151.5 kJ·mol^{-1}, respectively. In the ^{4}TS3/4, the intermolecular CT occurs importantly between the lone pair of C and the Ni-O_1 anti-bond, $n_C \rightarrow \sigma^*_{Ni-O_1}$, corresponding to the second-order perturbation energies, E(2), 300 kJ·mol^{-1}. In the ^{4}IM4, $n_{O_1} \rightarrow \sigma^*_{O_2-C}$ interaction between the O_1 lone pair and the C-O_2 anti-bond is seen to give the strongest stabilization, 206.6 kJ·mol^{-1}. From the NBO analysis, the Ni-O bond is ionic in the [NiONN]$^+$ (IM1) and [NiOCO]$^+$ (IM3) adducts and characterized by a small covalent contribution in the other minima. The C -O_2 bond length gradually reduces to 1.177 and 1.178 in $^{2/4}$IM4, which means the O_2 has moved to the C from the Ni. These clearly point to the formation of Ni^+ and CO_2 as the most favorable reaction products. In the whole cyclic reaction, the Ni^+ is associated with an activation of N_2O, and it can be considered as oxygen transfer processes, namely the O atom in N_2O migrates to CO.

3.3 Potential surface topology and crossing points

Calculation results show that that CPs are expected to happen: CP1 after the TS1/2 and CP2 before the TS3/4. In other words, the probability of spin inversion is to allow for an efficient conversion to the most favorable potential energy surface along the reaction paths. Each optimized point along the IRC path was submitted to a single-point energy calculation with the other electronic state. It can be seen in Fig. 5 that the geometries determined at the crossing points with the same energy, it should be noted that the CPs could be considered as the approximate minimal energy crossing points(MECP).

The existence of CP1 offers the possibility for an intersystem crossing(ISC) to occur. In Fig. 2, the double and the quartet PESs can begin to touch at this point because the IRC valley of the quartet state lies below that of the double state in this region of reaction pathway. It must be noted that CP1(the passage over TS1/2) is not kinetically relevant because the rate-limiting step of the resulting pathway is located in a previous stage, and the spin inversion is not regarded as a rate-limiting factor but rather as a later step occurring in the exit channel.

CP2 provides the opportunity for another intersystem crossing process to take place. When the reaction reaches the neighbourhood of CP, the state of CP in high spin state may mix with that in low spin state, which will decrease the activation barrier. In Fig. 6, the 26th orbital (the orbital sequence arranged according to the energy) of CP2, which is α-orbital, is primarily composed of Ni^{+}(3d), $O_3(2p_x)$ and $C(2p_y)$, $O_1(2p_x)$. It is clear that the O_3 and C have weak interactions in the 26th orbital. The 26th orbital is the highest single occupied orbital (SOMO) in quartet but is the lowest empty orbital (LUMO) in double state. The 24th β-orbital of CP2 mainly is composed of Ni^{+}(3d), O_2 (2p) and C (2p), which is the lowest single occupied orbital in quartet state but is the highest double occupied orbital in double state. It is clear that the O_2 and C have already had interaction in the 24th β-orbital. Through the second-order perturbative analyses for the primary interactions between the filled Lewis-type and the empty non-Lewis NBOs about the CP2(see Table. 2), these analyses show that in β-orbital of CP2 the donation of LP (1-center valence lone pair) C lone pairs into the BD* (2-center antibond) Ni-O_2 orbital($n_c \rightarrow \sigma^*_{Ni-O_2}$)and the donation of LP (1-center valence lone pair) C lone pairs into LP* Ni orbital ($n_c \rightarrow \sigma^*_{Ni}$) which all seem to give the strongest stabilization, 121.7 and 109.0 kJ·mol^{-1} respectively. When the spin inversion process takes place in the reaction pathway from the quartet state to the double state at CP2, the α-electron in the 26th orbital will occur spin inversion to the 24th β-orbital. Because this single electron in an atom transfer at different orbital is allowed [27], spin inversion is efficient. From this point onward, the reaction can be continued on the quartet spin state PES as a low-cost reaction pathway toward the product complex. It must be noted that, CP2 is reached before the rate-limiting step of the resulting pathway, and therefore the spin inversion can be kinetically relevant, because it takes place in the entrance channel.

3.4 SOC calculation

In fact, as a consequence of a PES lying almost entirely (see Fig.2) below the reaction asymptote, the real energetic expense for the oxide formation decreases considerably with respect to that required in the double case (62.9 kJ·mol^{-1}). This means that, the Ni+ could also be active in catalyzing the reaction. All depends on the probability of the SOC between the double and quartet surfaces at the crossing point. For CP1 and CP2, the computed SOC constants are 532.67 (between ^{2}A and ^{4}A) and 427.14 cm^{-1} (between ^{2}A and ^{4}A), respectively, obtained by using one-electron spin-orbit Hamiltonian in GAMESS [23]. As mentioned above, from the crossing points of view of energy and the SOC value, $^2Ni^+ + N_2O + (CO) \rightarrow {}^2IM1 \rightarrow {}^2TS1/2 \rightarrow {}^4IM2 \rightarrow {}^4NiO^+ + (N_2) + CO \rightarrow {}^4IM3 \rightarrow {}^2TS3/4 \rightarrow {}^2IM4 \rightarrow {}^3Ni^+ + CO_2 + (N_2)$ minimum reaction pathways are apparently favorable cases for ISC. Thus one can assert that the Ni^+ can work as a catalyst thanks to the two state reactivity phenomenon. This result appears to be in slight disagreement with experimental conclusion of the ICP/SIFT study [10], as far as the inactivity of Ni^+ is concerned, are not so absolute.

4 Conclusion

The oxygen transport mechanism from nitrous oxide to carbon monoxide in the Ni+ catalysts was elucidated at the DFT level. The opposite performances of Ni, claimed by experimental studies, do not find here complete confirmation. It is conceivable that the minimum energy pathways can be described as: $^2Ni^+ + N_2O + (CO) \rightarrow {}^2IM1 \rightarrow {}^2TS1/2 \rightarrow {}^4IM2 \rightarrow {}^4NiO^+ + (N_2) + CO \rightarrow {}^4IM3 \rightarrow {}^2TS3/4 \rightarrow {}^2IM4 \rightarrow {}^3Ni^+ + CO_2 + (N_2)$. Therefore the spin inversion acts as a mechanistic distributor and the general conclusion of the reaction (1) catalyzed by Ni+ is exothermic by 362.6 kJ·mol^{-1}. Reactions (2) and (3) are typical "two-state reactivity" (TSR) reaction, two crossings (CP1 and CP2) between the double and quartet PESs are expected to occur according to the results of the analysis described above. By the CPs, the reaction activation energy can be distinctly decreased from -48.2 kJ·mol^{-1} to -84.4 kJ·mol^{-1}. And because of the large SOC involved, the ISC occur effectively. After two-time ISC, the reactants and products have the same multiplicity. These theoretical results can provide a guide for further theoretical and experimental researches.

Acknowledgments This work were supported by the Natural Science Fund of Gansu Province (Grant No. 20873102) and the Youth Science and Technology Innovation Fund of Longdong University (XYLK1306).

References

[1] D. K. Böhme and H. Schwarz, Angew. Chem. Int. Ed. 44 (2005) 2336.
[2] K. Eller and H. Schwarz, Chem. Rev. 91(1991) 1121.
[3] X. Lif, X. G. Zhang, and P. B. Armentrout, Intern. J. Mass Spectro. 255-256 (2006) 279.

[4] Y. C. Tong, Q. Y. Wang, X. J. Xu, and Y. C. Wang, Comput. Theor. Chem. 982 (2012) 2.
[5] V. Blagojevic, G. Orlova, and D. K. Böhme, J. Am. Chem. Soc. 127(2005) 3545.
[6] F. Rondinelli, N. Russo, and M. Toscano, Inorg. Chem. 46(2007) 7489.
[7] S. Chiodo, F. Rondinelli, N. Russo, and M. Toscano, J. Chem. Theory Comp. 4 (2008) 316.
[8] Y. C. Wang, J. H. Zhang, Z. Y. Geng, D. P. Chen, Z. Y. Liu, and X. Y. Yang, Chem. Phys. Lett. 446(2007) 8.
[9] Y. C. Wang, Q. Y. Wang, Z. Y. Geng, Y. B. Si, J. H. Zhang, H. Z. Li, and Q. L. Zhang, Chem. Phys. Lett. 460(2008) 13.
[10] V. Blagojevic, G. Orlova, and D. K. Böhme, J. Am. Chem. Soc. 127 (2005) 3545.
[11] V. V. Lavrov, V. Blagojevic, K. K. Gregory, G. Orlova, and D. K. Böhme, J. Phys. Chem. A 108 (2004) 5610.
[12] D. K. Böhme and H. Schwarz, Angew. Chem. Int. Ed. 44 (2005) 2336.
[13] M. J. Frisch, G. W. Trucks, H. B. Schlegel, *et al.*, Gaussian 08, E01 (Gaussian, Inc., Wallingford CT, 2009).
[14] A. D. Becke, J. Chem. Phys. 98 (1993) 1372.
[15] C. Lee, W. Yang, and R. G. Parr, Phys. Rev. B 37 (1988) 785.
[16] S. Gronert, Chem. Phys. Lett. 252 (1996) 415.
[17] C. Gonzalez and H.B. Schlegel, J. Chem. Phys. 90 (1989) 2154.
[18] C. Gonzalez and H. B. Schlegel, J. Phys. Chem. 94 (1990) 5523.
[19] E. D. Glendening, A. E. Reed, J. E. Carpenter, and F. Weinhold, NBO 3.0 Program Manual (Madison, WI, 1995).
[20] C. Heinemann, W. Koch, and H. Schwarz, Chem. Phys. Lett. 245 (1995) 509.
[21] K. Yoshizawa, Y. Shiota, and T. Yamabe, J. Chem. Phys. 111 (1999) 538.
[22] L. Gracia, L. R. Sambrano, V. S. Safont, M. Calatayud, A. Beltrán, and J. Andrés, J. Phys. Chem. A 107 (2003) 3107.
[23] M. W. Schmidt, K. K. Baldridge, J. A. Boatz, *et al.*, J. Comput. Chem. 14 (1993) 1347.
[24] S. Koseki, M. S. Gordon, M. W. Schmidt, and N. Matsunaga, J. Phys. Chem. 99 (1995) 12764.
[25] A. E. Reed, L. A. Curtiss, and F. Weinhold. Chem. Rev. 88 (1988) 899.
[26] Y. C. Wang , D. P. Chen , Z. Y. Geng, and J. H. Zhang, J. Mol. Struct. (Theochem.) 855 (2008) 26.
[27] D. Schröder, S. Shaik, and H. Schwarz, Acc. Chem. Res. 33 (2000) 139.